Ultrasonics - Sonochemistry 48 (2018) 412–417

Contents lists available at ScienceDirect

Ultrasonics - Sonochemistry

journal homepage: www.elsevier.com/locate/ultson

Short communication

Ultrasonic-assisted synthesis of graphene oxide – fungal hyphae: An efficient and reclaimable adsorbent for chromium(VI) removal from aqueous solution

Melvin S. Samuel[a], Vasudevan Subramaniyan[b], Jayanta Bhattacharya[a], Ramalingam Chidambaram[c], Tanvir Qureshi[d], N.D. Pradeep Singh[b,*]

[a] School of Environmental Science and Engineering, Indian Institute of Technology, Kharagpur, West Bengal 721302, India
[b] Department of Chemistry, Indian Institute of Technology, Kharagpur, West Bengal 721302, India
[c] School of Bioscience and Technology, VIT University, Vellore 632014, Tamil Nadu, India
[d] Department of Civil Engineering, The University of Toronto, Toronto M5S 1A4, Ontario, Canada

ARTICLE INFO

Keywords:
Graphene oxide/funal hyphae (GO-FH)
Bio-nanocomposite
Ultrasonic
Chromium(VI)
Isotherm
Kinetics

ABSTRACT

In this study, a hybrid film bio-nanocomposite material was developed based on the graphene oxide/fungal hyphae (GO-FH) interaction. The developed GO-FH bio-nanocomposite material was used for the removal of hexavalent chromium from aqueous solution. The GO-FH bio-nanocomposite material was prepared by ultrasonic irradiation technique. The synthesized GO-FH bio-nanocomposite material was characterized by XRD, FT-IR, SEM, TEM and TGA. The adsorption experiments were carried out in batch mode to optimize parameters such as pH, adsorbent dosage, initial Cr(VI) ion concentration, contact time and shaking speed. The results indicated that the adsorption of Cr(VI) onto GO-FH bio-nanocomposite material was pH dependant, with the maximum adsorption capacity of 212.76 mg/g occurred at pH 2.0. The adsorption studies followed, Langmuir isotherm and pseudo second order kinetic model. Findings demonstrates that GO-FH bio-nanocomposite material exhibited excellent regeneration performance.

1. Introduction

The rapid evolution in industries have headed towards increased pollution, which is a major concern at present. Among the exiting heavy metals, chromium is a major toxic compound for the environment. Chromium enters in to water and soil through the discharge of waste from chemical factories, leather industries, steel, painting, coal combustion, electroplating and textile manufacturing [1]. These are the prime reason for the increase of chromium in the environment. Among the existing forms of chromium, Cr(VI) is more predominant and causes higher level of toxicity towards humans such as skin disease, ulcer, kidney and liver damages [2]. In current scenario, one of the most important economical task is to remove chromium concentration in the industrial wastewater under the tolerable limit < 1 mg/L [3]. Presently used conventional methods includes chemical precipitation [4], liquid-liquid extraction [5], ion-exchange and dialysis [6]. However, these methods are extremely expensive, ineffective at lower concentrations, requires expensive organic solvents, chemical reagents and also leads to environmental problems in terms of waste disposal [7–11].

The necessity to find cost effective and non-polluting approaches has directed towards the development of separation techniques. The naturally available materials such as tea leaves, peat, soils and clays provide greater adsorption but their main drawback arises in terms of regeneration capacity [12–14]. Some of the synthesized materials like zeolite, polymer coated materials, ionic hybrids and resin coated materials requires high fabrication cost. Nevertheless, these materials provide very good sorption capacity, greater selectivity and are easy to regenerate. A number of studies have been testified on metal binding capacity of several strains of bacteria, algae, fungi and sea weed [15–17]. Amongst the existing microbes, fungi contains higher amount of cell wall material which can be used for metal binding capacity [18–20]. The fungi cell wall is made up of chitin, amino carboxyl, hydroxyl, phosphoryl and imidazole groups [16,21–23]. Few studies reported on the mechanism of interaction between fungal biomass and Cr (VI) ions [16]. The dead fungal biomass binding with graphene oxide (GO) could be a source of material for Cr(VI) adsorption process. GO is a carbon material with greater specific surface area and extensive mechanical properties. GO contains functional groups such as hydroxyl, epoxy and carboxyl groups [24]. When it comes to adsorption technique, the oxygen containing functional group in the GO binds with the heavy metal ions through metal ions complexes [25]. Ultrasonic is currently used in diverse fields of nanochemistry and nanotechnology

* Corresponding author.
E-mail address: ndpradeep@chem.iitkgp.ernet.in (N.D. Pradeep Singh).

https://doi.org/10.1016/j.ultsonch.2018.06.012
Received 29 April 2018; Received in revised form 29 May 2018; Accepted 14 June 2018
Available online 20 June 2018
1350-4177/

[26]. The ultrasonic irradiation technique offers facile and it's an essential tool for developing nanostructured materials, which cannot be synthesized by existing conventional techniques [27,28]. The main advantage of this technique, is that it offers unusual reaction conditions such as high pressure and temperature in a short reaction time [29,30]. Ultrasonic irradiation in liquid medium induces pressure waves that generate cavities. Hence, this technique can be applied in the homogenization process [31].

In this study, a novel biomaterial using graphene oxide/fungal hyphae (GO-FH) bio-nanocomposite material was effectively synthesized and characterized by Fourier transform infrared spectroscopy (FT-IR), X-ray diffraction (XRD), scanning electron microscopy (SEM), transmission electron microscopy (TEM), thermal gravimetric analysis (TGA) and its Cr(VI) adsorption performances, involving the adsorption kinetics and isotherms were studied.

2. Materials and methods

2.1. Chemicals used

The natural graphite powder (purity, 99.0%), sodium nitrate ($NaNO_3$), potassium dichromate ($K_2Cr_2O_7$) potassium permanganate ($KMnO_4$), sulfuric acid (H_2SO_4) and 1,5-diphenylcarbazide (1,5-DPC) were reagent grade (Sigma–Aldrich). The acids and bases, hydrochloric acid (HCl) and sodium hydroxide (NaOH) were reagent grade.

2.2. Synthesis of GO-fungal hyphae loaded hybrid film

In this study, the detailed procedures of graphene oxide (GO) synthesis and preparation of fungal hyphae are given in Supporting information S1 Experimental section. To synthesize GO-FH bio-nanocomposite, 7.0 g of GO was dissolved in 40 mL of distilled water. Then, 1.0 g of dried MSR3 fungal biomass was added into the GO dispersed solution. The solution was stirred for 12 h at 27 °C and then it was sonicated for 3 h, with an input power 100 W and frequency 40 KHz (UR Biocoction Ultrasconic Co., Kolkata). An extended incubation time 3 h was chosen for the study. To remove the solvent, the resultant mixture solutions were poured into petri dishes and was placed in hot air oven at 60 °C for 2 days. Finally, the material (GO-FH bio-nanocomposite) was collected and allowed to cool naturally at room temperature.

2.3. Adsorbent characterization

Crystallographic patterns of graphite, GO, GO-FH bio-nanocomposite materials were assessed by XRD (Type: PW3040/60; S/N: DY3823) with a Cu tube anode, PANalytical (Made in Netherlands). FTIR spectrometer (Thermo Nicolet-870 spectrophotometer) was used to record the FTIR spectra ranging from 400 to 4000 cm^{-1} To investigate the morphology and size of the materials, SEM (Zeiss Auriga instrument) and TEM (Model: FEI-TECHNAI-G2 20 TWIN) was used. Thermal stability was measured with a TGA (Perkin Elmer Inc., Massachusetts, USA) at a heating rate of 10 °C min^{-1} from 0 to 800 °C.

2.4. Adsorption experiments

The Cr(VI) removal over GO-FH bio-nanocomposite material were studied in batch experiments. To attain the optimum conditions for removal of Cr(VI), the effect of pH (1.0–9.0), contact time (0–600 min), shaking speed (60–120 rpm), adsorbent dosage (0.125–1.0 g/L) were studied. The adsorption experiments were performed in 20 mL flask containing 10 mL of Cr(VI) solution at various concentrations (10–125 mg/L) was equipped by suitable dilutions of the stock solution. The pH of the stock solution was adjusted to pH 2.0 and 0.5 g/L of GO-FH bio-nanocomposite material was added. After the equilibrium time, the adsorbents were filtered and the residual Cr(VI) concentrations were assessed by 1,5-diphenylcarbazide method in a UV visible spectrophotometer at λ_{max} = 540 nm. The adsorption capacity of Cr (VI) was evaluated by the subsequent equation (1).

$$q_e = \frac{C_O - C_f}{M} \times V \tag{1}$$

$$\%\, removal = \frac{C_0 - C_f}{C_0} \times 100 \tag{2}$$

where C_o and C_f are the initial and equilibrium concentration of Cr(VI) respectively. V (L) is the volume of the solution, m(g) is the weight of the adsorbent and q_e (mg/g) is the adsorption capacity of the adsorbent. In order to describe the adsorption process, pseudo-first order and pseudo-second order models were employed. To determine the adsorption equilibrium Langmuir and Freundlich isotherm models were applied in our study. The Langmuir adsorption model can be expressed by Eqs. (3) and (4) as nonlinear and linear forms, respectively.

$$q_e = \frac{q_{\max} b C_{eq}}{1 + bC_{eq}} \tag{3}$$

$$\frac{1}{q_e} = \frac{1}{q_{\max}} + \frac{1}{q_{\max} b} \frac{1}{C_{eq}} \tag{4}$$

where, q_e is the metal concentration adsorbed, C_{eq} is the remaining metal residual in solution, q_{max} is the maximum uptake with respect to adsorption sites saturation and b is the ratio of the adsorption/desorption rate.

The Langmuir isotherm can be described by a dimensionless equilibrium parameter R_L and determined by Eq. (5). Where R_L is known as separation factor and it is used for the applicability of adsorption process. If $R_L < 1$, implies the favourable adsorption; $R_L = 0$ implies the adsorption process is irreversible; $R_L > 1$ implies the adsorption process is unfavourable and if $R_L = 1$ implies the adsorption process is linear.

$$R_L = \frac{1}{1 + K_L C_o} \tag{5}$$

The Freundlich adsorption isotherm is expressed in Eq. (6) and its linearized form is given in Eq. (7), here K and n are constants. Where C_{eq} is related to adsorption capacity and n is given as adsorption intensity.

$$q_e = K_f C_e^{1/n} \tag{6}$$

$$\log q_e = \log K_f + \frac{1}{n} \log C_e \tag{7}$$

Kinetic models are used for determining the adsorption mechanism in batch studies. The rate of Cr(VI) removal by GO-FH bio-nanocomposite material was studied using three different kinetic models *viz.*, pseudo-first order and pseudo-second order. The above mentioned kinetic models and their equations are given below:

$$\log (q_e - q_t) = \log q_{eq} - \frac{Kt}{2.303} \tag{8}$$

$$\frac{t}{q_t} = \frac{1}{Kq_e^2} + \frac{1}{q_e} t \tag{9}$$

where, q_e is the amount of adsorbate (mg) adsorbed per unit mass (g) of adsorbent at equilibrium, q_t is the amount of adsorbate (mg) adsorbed per unit mass (g) of adsorbent at time t, K_1 is the rate constant (1/min) for pseudo first order reaction and K_2 is the rate constant (g/mg/min) for pseudo second order reaction.

3. Results and discussion

3.1. Adsorbent characterization

3.1.1. Powder X-ray diffraction (PXRD) and Fourier transform infrared spectroscopy (FTIR)

The PXRD spectra of graphite, graphene oxide and GO-FH bio-nanocomposite material were shown in Fig S1a†. The distinctive peaks of graphite, GO appeared at 2Θ = 26.4° and 9.56°, respectively. A distinguished peak at 2 Θ = 9.56° indicated the successful conversion from graphite to GO [32]. Whereas, GO-FH bio-nanocomposite material exhibited a small peak at 9.56°, signifying the existence of GO. The FT-IR analysis was done for GO, fungus and GO-FH bio-nanocomposite material are shown in Fig S1b†. The GO adsorption peaks at 3302 cm^{-1}, 1734 cm^{-1}, 1624 cm^{-1} and 1058 cm^{-1} corresponds to the stretching vibrations of OH, C═O, C—C vibrations of graphene oxide. The peaks at 1410 cm^{-1}, 1240 cm^{-1} and 1058 cm^{-1} are the peaks assigned for carboxyl (C═O), epoxy (C—O) and alkoxy (C—O) vibrations, respectively. The FT-IR spectra of fungal hyphae showed the distinctive peaks at 3439 cm^{-1} (OH vibrations). The absorption peak at 1644 cm^{-1}, 1404 cm^{-1} and 1262 cm^{-1} should be due to the vibrations of the amide of protein and chitin. The peak at 1094 cm^{-1} is due to polysaccharides. Compared to the FT-IR spectra of the two parental material, the intense peak of oxygen containing group in the GO-FH bio-nanocomposite material decreased significantly is shown in Fig. S1b†. It has to be noted that only a slight intensity differences observed in the GO-FH bio-nanocomposite material and fungal hyphae. The peak observed at 1262 cm^{-1} in the GO-FH bio-nanocomposite material is cause by the fungal hyphae, which is due to the cross linking interaction between fungal hyphae and GO.

3.1.2. SEM and TEM analysis

The surface structure of the materials was analysed by SEM. The SEM image of fungal hyphae, graphene oxide and GO-FH bio-nanocomposite material are shown in Fig. 1. The fungal hyphae composed of fibre like materials, with regular smooth colonies are shown in Fig. 1(a and b). The GO image shown a porous, homogeneous and consistent structure is shown in Fig. 1c. While, the morphology of GO-FH bio-nanocomposite material becomes rougher, non-homogeneous and rough surface denotes the mounting of fungal hyphae onto GO planes are shown in Fig. 1d. Similarly, TEM image of GO and GO-FH bio-nanocomposite material are shown in Fig. 2. The TEM image of GO exhibits a clear and linear distribution (Fig. 2a). The TEM image of GO-

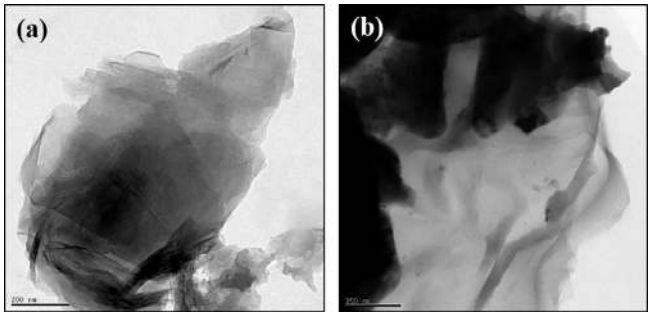

Fig. 2. TEM images of materials (a) GO, (b) GO-FH bio-nanocomposite material.

Table 1
Isotherm model regression constants for different experimental conditions.

Isotherm models	Parameters	0.125 g/L	0.25 g/L	0.5 g/L	1.0 g/L
Langmuir	q_{max} (mg/g)	212.76	142.85	103.09	81.3
	K_L (L/mg)	0.124	0.09	0.088	0.036
	R^2	0.9839	0.9914	0.9984	0.983
Freundlich	K_f (mg/g)	50.52	25.79	21.31	13.43
	N	3.146	2.719	2.169	2.695
	R^2	0.8696	0.9685	0.9511	0.7694

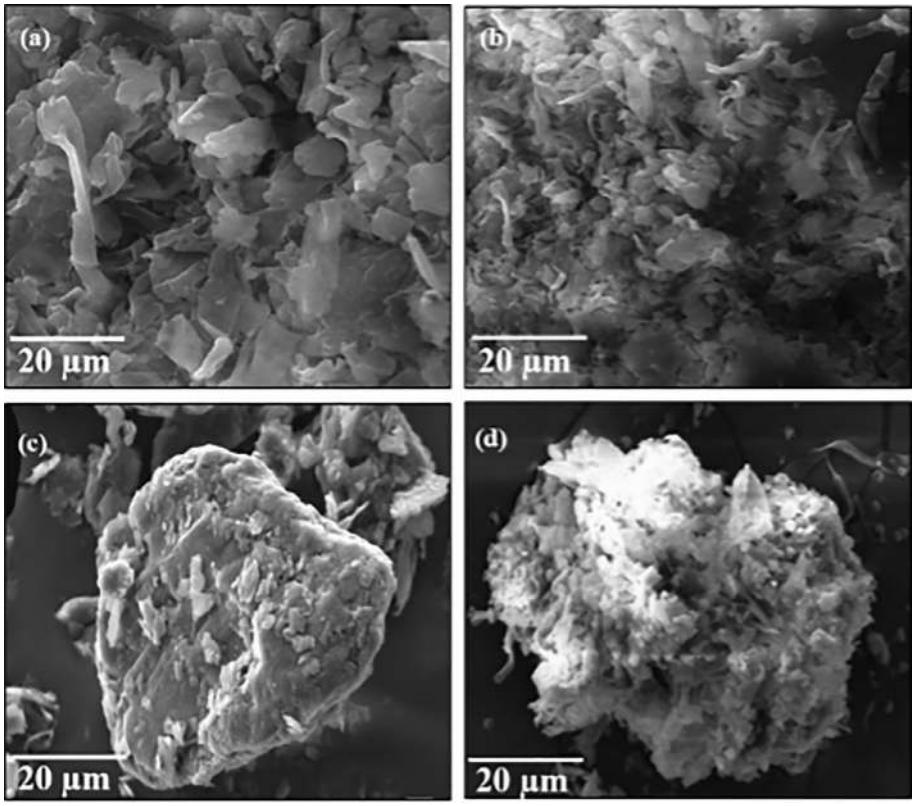

Fig. 1. SEM images of materials (a, b) Fungus, (c) GO, (d) GO-FH bio-nanocomposite material.

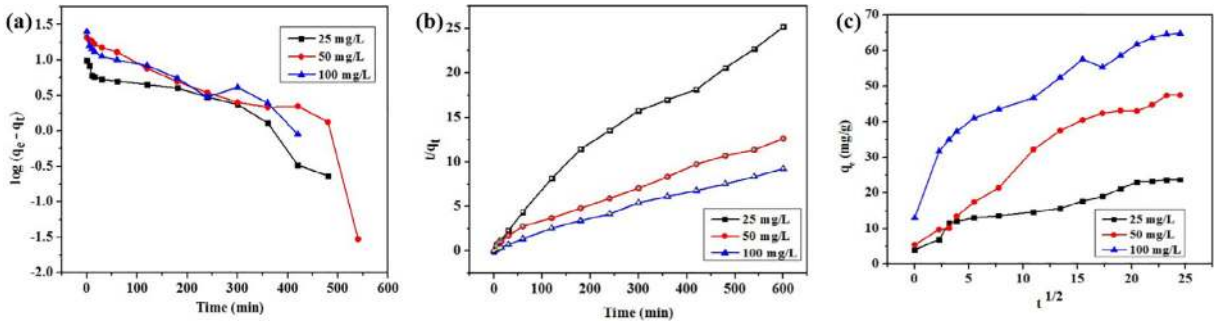

Fig. 3. Kinetic modelling of the adsorption of Cr(VI) on GO-FH bio-nanocomposite material, (a) pseudo first order kinetic plot, (b) pseudo second order kinetic; (c) intraparticle diffusion plot.

Table 2
Kinetics parameters for the adsorption of Cr(VI) by GO-FH bio-nanocomposite material based on different concentrations.

Concentration (mg/L)	25	50	100
Pseudo- first order			
K_1 (min^{-1})	6.2181×10^{-3}	7.8302×10^{-3}	7.36×10^{-3}
q_e (mg/g)	32.99	86.15	73.65
R^2	0.9361	0.8301	0.9459
Pseudo– second order			
K_2 (min^{-1})	0.028	0.022	0.045
q_e (mg/g)	48.54	100	129.87
R^2	0.9824	0.991	0.9931
Intraparticle diffusion			
R_{id}	1.439	3.637	3.381
C	14.79	15.09	54.40
R^2	0.9473	0.9574	0.9047

Table 3
Adsorption comparison of CS-GO and reported studies on adsorbents for Cr(VI).

S. No.	Adsorbent material	q_{max} (mg/g)	Reference
1	Ethylenediamine-modified cross-linked magnetic chitosan	51.813	[37]
2	Chitosan	22.09	[34]
3	Graphene nanosheets	43	[38]
4	Chitosan cross-linked with epichlorohydrin	52.3	[39]
5	Magnetic chitosan nanoparticle	55.8	[40]
6	$MnFe_2O_4$-chitosan	15.4	[41]
7	PANI/H-TNB composites	156.94	[42]
8	PVP/MoS_2	142.24	[43]
9	Magnetic porous carbonaceous (MPC)	21.23	[44]
10	GO-FH bio-nanocomposite material	212.76	**This study**

FH bio-nanocomposite material exhibits an irregular, rough surface and non-homogenous nature. This confirms the mounting of fungal hyphae upon GO layer (Fig. 2b).

3.1.3. Thermogravimetric analysis

The TGA analysis was done for the prepared GO and GO-FH bio-nanocomposite material and the weight loss curves are presented in Fig. S2†. The GO showed a significant drop in weight at two places at around 80 °C and 200 °C. The first weight loss is due to the elimination of adsorbed water molecules on GO sheets. The second weight loss, occurs at 200 °C, which is due to the removal of oxygenated functional groups of GO (*i.e.* C═O, C—O—C and —OH). Whereas, the GO-FH bio-nanocomposite material showed a weight loss at four places. The first weight loss appears around 90–100 °C corresponds to loss of water. The second one emerges around 305 °C must be due to the decomposition of chitin molecule [33]. The third weight loss occurs in the range of 530 °C must be due to deacetylation of polymer chain and breakage of glycosidic linkages. The final weight loss at 670 °C is due to the thermal annihilation of pyranose ring and decay of the remaining carbon [33]. In comparison GO showed higher weight loss than the GO-FH bio-nanocomposite material. Hence, GO-FH bio-nanocomposite material showed better stability than the GO material.

3.2. Effect of various parameters

The influence of pH on Cr(VI) removal by GO-FH bio-nanocomposite material was evaluated. For this study, a varied range of pH (1.0–9.0) was chosen and it was found that the Cr(VI) adsorption increases significantly with decrease in pH (< 4.0) and the adsorption capacity of Cr(VI) decreases with increase in pH above 4.0. The maximum adsorption capacity was achieved at pH 2.0. The pH_{zpc} of the GO-FH bio-nanocomposite material was found to be 8.0 is shown in Fig. S3†. The effect of adsorbent dosage on Cr(VI) removal by GO-FH bio-nanocomposite material was examined. The removal rate of Cr(VI) onto GO-FH bio-nanocomposite material increased gradually with the

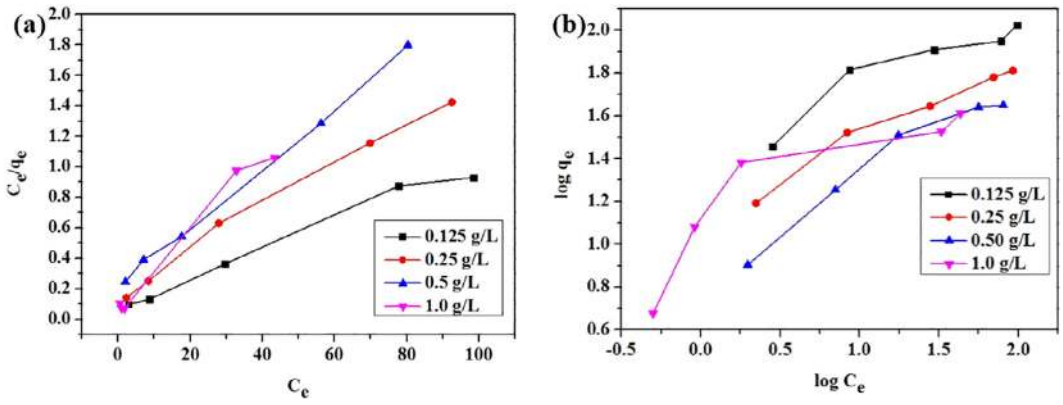

Fig. 4. (a) Langmuir isotherm plot, (b) Freundlich isotherm plot for removal of Cr(VI) by GO-FH bio-nanocomposite material.

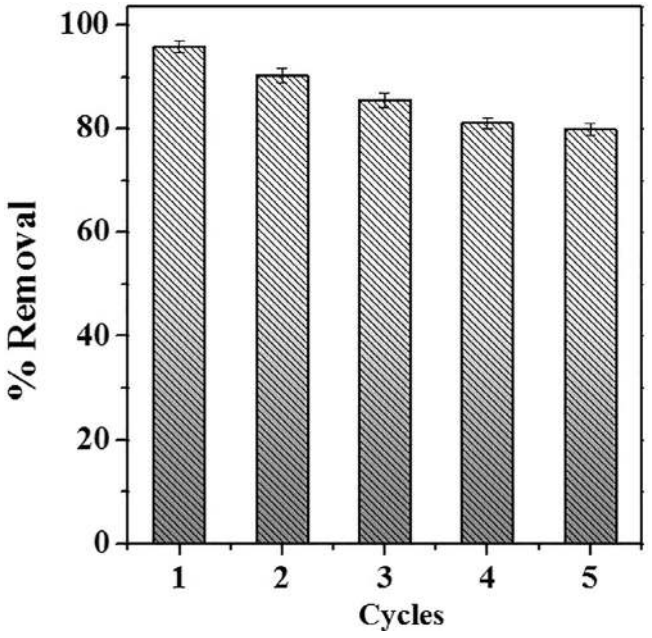

Fig. 5. Regeneration study of GO-FH bio-nanocomposite within five cycles.

increase of adsorbent dose from 0.125 to 1.0 g/L. Whereas, the adsorbent capacity of Cr(VI) on GO-FH bio-nanocomposite material decreased from 212.76 mg/g to 81.3 mg/g as the adsorbent dosage increasing from 0.125 g/L to 1.0 g/L (Table. 1). The effect of contact time on the removal of Cr(VI) by GO-FH bio-nanocomposite material was investigated at three different Cr(VI) concentrations (25, 50 and 100 mg/L). Time chosen for this study was 0–600 min with the dose of 0.5 g/L at temperature 27 °C and agitation speed of 120 rpm. At lower concentrations (50 mg/L) the maximum Cr(VI) adsorption occurred within 540 min, showing 97% removal (Fig. S4†). The amount of Cr(VI) adsorbed onto GO-FH bio-nanocomposite material increases with the increase in contact time, this is mainly due to the availability large number available spots for adsorption. After the 540 min the adsorption capacity of GO-FH bio-nanocomposite material reaches equilibrium state. The effect of agitation speed on the removal of Cr(VI) by GO-FH bio-nanocomposite material was studied by shaking the 50 mg/L of Cr (VI) sample (10 mL) at different agitation speeds viz., 60, 80, 100 and 120 rpm. The other parameters such as pH (2.0), incubation time (540 min) and adsorbent dosage (0.5 g/L) were kept constant. The results have shown that an increase in shaking speed from 60 to 140 rpm, the removal of Cr(VI) also increases as shown in Fig. S5†. From the above result, 120 rpm was selected as the optimal shaking speed for further experiments.

3.3. Kinetic and adsorption isotherm studies

The kinetics studies were performed in varying Cr(VI) concentrations (25, 50 and 100 mg/L) using GO-FH bio-nanocomposite material and the results are shown in Fig. 3. Three kinetic models such as pseudo first order, pseudo second order kinetic models and intra-particle diffusion model were used (Fig. 3). The calculated results are given in Table 2. The R^2 value of the pseudo second order model was found to be better than those of the other two models (Table 2). The calculated q_e values of the pseudo second order model is in accordance with the experimental q_e values. The Cr(VI) uptake process follows the pseudo second order kinetic reaction. Similarly, we have also calculated the intra-particle diffusion, which indicates low R^2 value and non-linear plot, similarly reported in other studies. The adsorption isotherm of Cr (VI) were examined at different adsorbent dosage levels (0.125–1.0 g/L) using Langmuir and Freundlich isotherm models (Fig. 4). The Langmuir model depicts monolayer surface adsorption. Whereas, the Freundlich model assumes the heterogeneous mode of adsorption without saturation of adsorbent binding sites. The experimental data are fitted to both Langmuir and Freundlich isotherm model. However, based on the correlation coefficients (R^2) and fitting curves, the Langmuir isotherm model is a best fit and it indicates the surface of GO-FH bio-nanocomposite material is likely to be homogenous nature. The maximum adsorption capacity was 212.76 mg/g (Table 1), which is quite higher in comparison to some of the early reported adsorbents (Table 3). The prepared GO-FH bio-nanocomposite material was compared with the other reported q_{max} values which are shown in the Table 3. It was found that, the GO-FH bio-nanocomposite material showed the Langmuir adsorption capacity of 212.76 mg/g, which is better than the other adsorbents. It is shown in the table that the pure chitosan showed only 22.09 mg/g [34], while the modified form of chitosan like cyclodextrin–chitosan modified GO (61.31 mg/g) [35], magnetic chitosan-GO nanoparticle (82.14 mg/g) [36] and CS-GO (104.16 mg/g) showed better adsorption.

3.4. Adsorption regeneration and reuse

The Cr(VI) desorption study was carried out with 1 mol L^{-1} NaOH, after desorbing the Cr(VI) from GO-FH bio-nanocomposite material. The same material was used again for the successive adsorption studies and the material adsorption capacity was checked. It was found that GO-FH bio-nanocomposite material was able to adsorb Cr(VI) from aqueous solution up to five cycle with very less decrease in adsorption capacity. It can be seen in the graph (Fig. 5) that GO-FH bio-nanocomposite material after five cycles showed 80% removal efficiency. The removal rate decreased marginally from 97% first cycle to 80% fifth cycles. The results validate that GO-FH bio-nanocomposite material can be economically effective in adsorbing Cr(VI) ions from waste water.

4. Conclusion

The GO-FH bio-nanocomposite material was synthesized and characterized by SEM, TEM, XRD, FT-IR and TGA. The XRD and FT-IR data showed the presence of GO, amino and carboxyl groups in the GO-FH bio-nanocomposite material. The surface morphology of the GO-FH bio-nanocomposite material were investigated by SEM and TEM. TGA data revealed the improvement in thermal stability of the GO-FH bio-nanocomposite material. The adsorption capacity of GO-FH bio-nanocomposite material was found to be dependent on the pH and initial Cr (VI) concentration of solution. Maximum percentage removal (97%) of Cr(VI) occurred at pH -2.0, concentration of 50 mg/L, contact time 540 min, which decreased to 80% after five cycle. The equilibrium and kinetic data revealed the suitability of Langmuir isotherm and pseudo second order for defining the adsorption process of GO-FH bio-nanocomposite material. The experimental sorption data best fits to Langmuir isotherm model and maximum sorption capacity was found to be 212.76 mg/g. This study validates that the GO-FH bio-nanocomposite material could be used as a low-cost and highly efficient adsorbing agent for the removal of heavy metals from contaminated aqueous solutions.

Acknowledgement

Dr. Melvin Samuel. S is deeply thankful to School of Environmental Science and Engineering, Indian Institute of Technology Kharagpur for the fellowship.

Appendix A. Supplementary data

Supplementary data associated with this article can be found, in the online version, at https://doi.org/10.1016/j.ultsonch.2018.06.012.

References

[1] C.A. Kozlowski, W. Walkowiak, Applicability of liquid membranes in chromium(VI) transport with amines as ion carriers, J. Memb. Sci. 266 (2005) 143–150.

[2] D.A. Kimborough, Y. Cohen, A.M. Winer, L. Creelman, C. Mabuni, A critical assessment of chromium in the environment, Crit. Eviews Environ. Sci. Technol. 29 (1999) 1–46.

[3] A. Zouhri, B. Ernst, M. Burgard, Bulk liquid membrane for the recovery of chromium(VI) from a hydrochloric acid medium using dicyclohexano-18-crown-6 as extractant-carrier, Sep. Sci. Technol. 34 (1999) 1891–1905.

[4] J. Liu, H. Chen, X. Mao, X. Jin, Determination of trace copper, lead, cadmium, and iron in environmental and biological samples by flame atomic absorption spectrometry coupled to flow injection on-line coprecipitation preconcentration using DDTC-nickel as coprecipitate carrier, Int. J. Environ. Anal. Chem. 76 (2000) 267–282.

[5] D. Bonam, G. Bhattacharyya, A. Bhowal, S. Datta, Liquid – Liquid extraction in a rotating-spray column: removal of Cr(VI) by, Ind. Eng. Chem. Res. 48 (2009) 7687–7693.

[6] R. Navarro, I. Saucedo, A. Núñez, M. Ávila, E. Guibal, Cadmium extraction from hydrochloric acid solutions using Amberlite XAD-7 impregnated with Cyanex 921 (tri-octyl phosphine oxide), React. Funct. Polym. 68 (2008) 557–571.

[7] S. Karthikeyan, V.K. Gupta, R. Boopathy, A. Titus, G. Sekaran, A new approach for the degradation of high concentration of aromatic amine by heterocatalytic Fenton oxidation: kinetic and spectroscopic studies, J. Mol. Liq. 173 (2012) 153–163.

[8] K.A. Mocniak, I. Kubajewska, D.E.M. Spillane, G.R. Williams, R.E. Morris, Incorporation of cisplatin into the metal–organic frameworks UiO66-NH 2 and UiO66 – encapsulation vs. conjugation, RSC Adv. 5 (2015) 83648–83656.

[9] V.K. Gupta, R. Jain, A. Mittal, T.A. Saleh, A. Nayak, S. Agarwal, S. Sikarwar, Photocatalytic degradation of toxic dye amaranth on TiO2/UV in aqueous suspensions, Mater. Sci. Eng. C. 32 (2012) 12–17.

[10] R. Saravanan, M.M. Khan, V. Kumar, E. Mosquera, F. Gracia, V. Narayanan, A. Stephen, ZnO/Ag/CdO nanocomposite for visible light-induced photocatalytic degradation of industrial textile effluents, J. Colloid Interface Sci. 452 (2015) 126–133.

[11] D. Robati, B. Mirza, M. Rajabi, O. Moradi, I. Tyagi, S. Agarwal, V.K. Gupta, Removal of hazardous dyes-BR 12 and methyl orange using graphene oxide as an adsorbent from aqueous phase, Chem. Eng. J. 284 (2016) 687–697.

[12] G.P. Dasmahapatra, T.K. Pal, B. Bhattacharya, Continuous separation of hexavalent chromium in a packed bed of flyash pellets, Chem. Eng. Technol. 21 (1998) 89–95.

[13] E. Malkoc, Y. Nuhoglu, Determination of kinetic and equilibrium parameters of the batch adsorption of Cr(VI) onto waste acorn of Quercus ithaburensis, Chem. Eng. Process. Process Intensif. 46 (2007) 1020–1029.

[14] S. Mor, K. Ravindra, N.R. Bishnoi, Adsorption of chromium from aqueous solution by activated alumina and activated charcoal, Bioresour. Technol. 98 (2007) 954–957.

[15] H. Javadian, M. Ahmadi, M. Ghiasvand, S. Kahrizi, R. Katal, Removal of Cr (VI) by modified brown algae Sargassum bevanom from aqueous solution and industrial wastewater, J. Taiwan Inst. Chem. Eng. 44 (2013) 977–989, http://dx.doi.org/10.1016/j.jtice.2013.03.008.

[16] J. Wang, C. Chen, Biosorbents for heavy metals removal and their future, Biotechnol. Adv. 27 (2009) 195–226.

[17] B. Van der Bruggen, C. Vandecasteele, Removal of pollutants from surface water and groundwater by nanofiltration: overview of possible applications in the drinking water industry, Environ. Pollut. 122 (2003) 435–445.

[18] H. Rezaei, Biosorption of chromium by using Spirulina sp, Arab. J. Chem. 9 (2016) 846–853.

[19] L. Ramrakhiani, R. Majumder, S. Khowala, Removal of hexavalent chromium by heat inactivated fungal biomass of termitomyces clypeatus: surface characterization and mechanism of biosorption, Chem. Eng. J. 171 (2011) 1060–1068.

[20] Y.L. Chen, X.Q. Hong, H. He, H.W. Luo, T.T. Qian, R.Z. Li, H. Jiang, H.Q. Yu, Biosorption of Cr(VI) by typha angustifolia: mechanism and responses to heavy metal stress, Bioresour. Technol. 160 (2014) 89–92.

[21] N.Z. Zhou, P. Liu, X.C. Su, Y.H. Liao, N.S. Lei, Y.H. Liang, S.H. Zhou, W.S. Lin, J. Chen, Y.Q. Feng, Y. Tang, Low-cost humic acid-bonded silica as an effective solid-phase extraction sorbent for convenient determination of aflatoxins in edible oils, Anal. Chim. Acta. 970 (2017) 38–46.

[22] L. Prasanna, J. Reddy, Y. Choi, Hydrometallurgy Studies on removal of Pb (II) and Cr (III) using graphene oxide based inverse spinel nickel ferrite nano-composite as sorbent, Hydrometallurgy 165 (2015) 64–72, http://dx.doi.org/10.1016/j.hydromet.2015.11.005.

[23] H. Li, L. Zhang, Z. Sun, Y. Liu, B. Yang, S. Yan, One-step synthesis of magnetic 1,6-hexanediamine-functionalized reduced graphene oxide–zinc ferrite for fast adsorption of Cr(< scp > vi < /scp >), RSC Adv. 5 (2015) 31787–31797.

[24] N. Cai, P. Larese-Casanova, Application of positively-charged ethylenediamine-functionalized graphene for the sorption of anionic organic contaminants from water, J. Environ. Chem. Eng. 4 (2016) 2941–2951, http://dx.doi.org/10.1016/j.jece.2016.06.004.

[25] S. Luo, X. Xu, G. Zhou, C. Liu, Y. Tang, Y. Liu, Amino siloxane oligomer-linked graphene oxide as an efficient adsorbent for removal of Pb(II) from wastewater, J. Hazard. Mater. 274 (2014) 145–155.

[26] A. Hassani, G. Çelikdağ, P. Eghbali, M. Sevim, S. Karaca, Ö. Metin, Heterogeneous sono-Fenton-like process using magnetic cobalt ferrite-reduced graphene oxide (CoFe 2 O 4 -rGO) nanocomposite for the removal of organic dyes from aqueous solution, Ultrason. Sonochem. 40 (2018) 841–852.

[27] M. Safarpoor, M. Yousefinejad, M. Ghaedi, H. Zare Khafri, A. Asfaram, M. Bagherinasab, M. Kocheki Shahmokhtar, Ultrasound-assisted extraction of antimicrobial compounds from thymus daenensis and silybum marianum and investigation of its in presence and without of natural silver nanoparticles, Nat. Prod. Chem. Res. 05 (2017) 76–83.

[28] S. Zhu, J. Guo, J. Dong, Z. Cui, T. Lu, C. Zhu, D. Zhang, J. Ma, Sonochemical fabrication of Fe_3O_4 nanoparticles on reduced graphene oxide for biosensors, Ultrason. Sonochem. 20 (2013) 872–880.

[29] V. Vinoth, J.J. Wu, A.M. Asiri, S. Anandan, Sonochemical synthesis of silver nanoparticles anchored reduced graphene oxide nanosheets for selective and sensitive detection of glutathione, Ultrason. Sonochem. 39 (2017) 363–373.

[30] Y. Areerob, C.J. Yong, J.W. Kweon, W.-C. Oh, Enhanced sonocatalytic degradation of organic dyes from aqueous solutions by novel synthesis of mesoporous Fe_3O_4 -graphene/ZnO@SiO_2 nanocomposites, Ultrason. Sonochem. 41 (2017) 267–278.

[31] A.R. Bagheri, M. Ghaedi, A. Asfaram, A.A. Bazrafshan, R. Jannesar, Comparative study on ultrasonic assisted adsorption of dyes from single system onto Fe_3O_4 magnetite nanoparticles loaded on activated carbon: Experimental design methodology, Ultrason. Sonochem. 34 (2017) 294–304.

[32] Z. Li, H. Luo, P. Liu, W. Fang, J. Geng, A novel modified graphene oxide/chitosan composite used as an adsorbent for Cr(VI) in aqueous solutions, Int. J. Biol. Macromol. 87 (2016) 586–596, http://dx.doi.org/10.1016/j.ijbiomac.2016.03.027.

[33] X. Sun, B. Peng, Y. Ji, J. Chen, D. Li, Chitosan(chitin)/cellulose composite biosorbents prepared using ionic liquid for heavy metal ions adsorption, AICHE J. 55 (2009) 2062–2069 (accessed July 28, 2017), http://doi.wiley.com/10.1002/aic.11797.

[34] Y.A. Aydin, N.D. Aksoy, Adsorption of chromium on chitosan: optimization, kinetics and thermodynamics, Chem. Eng. J. 151 (2009) 188–194.

[35] L. Li, L. Fan, M. Sun, H. Qiu, X. Li, H. Duan, C. Luo, Colloids and surfaces B: biointerfaces adsorbent for chromium removal based on graphene oxide functionalized with magnetic cyclodextrin–chitosan, Colloids Surfaces B Biointerfaces 107 (2013) 76–83, http://dx.doi.org/10.1016/j.colsurfb.2013.01.074.

[36] S. Debnath, A. Maity, K. Pillay, Magnetic chitosan – GO nanocomposite: synthesis, characterization and batch adsorber design for Cr(VI) removal, J. Environ. Chem. Eng. 2 (2014) 963–973.

[37] X. Jiang Hu, J. Song Wang, Y. Guo Liu, X. Li, G. Ming Zeng, Z. Lei Bao, X. Xia Zeng, A. Wei Chen, F. Long, Adsorption of chromium (VI) by ethylenediamine-modified cross-linked magnetic chitosan resin: Isotherms, kinetics and thermodynamics, J. Hazard. Mater. 185 (2011) 306–314.

[38] H. Jabeen, V. Chandra, S. Jung, J.W. Lee, K.S. Kim, S. Bin Kim, Enhanced Cr(vi) removal using iron nanoparticle decorated graphene, Nanoscale 3 (2011) 3583–3585.

[39] T. Tianwei, H. Xiaojing, D. Weixia, Adsorption behaviour of metal ions on imprinted chitosan resin, J. Chem. Technol. Biotechnol. 76 (2001) 191–195.

[40] N.N. Thinh, P.T.B. Hanh, T.V. Hoang, V.D. Hoang, L.H. Dang, N. Van Khoi, T. Dai, Lam, Magnetic chitosan nanoparticles for removal of Cr (VI) from aqueous solution, Mater. Sci. Eng. C. 33 (2013) 1214–1218.

[41] A.Z.M. Badruddoza, Z.B.Z. Shawon, W.J.D. Tay, K. Hidajat, M.S. Uddin, Fe_3O_4/cyclodextrin polymer nanocomposites for selective heavy metals removal from industrial wastewater, Carbohydr. Polym. 91 (2013) 322–332.

[42] T. Wen, Q. Fan, X. Tan, Y. Chen, C. Chen, A. Xu, X. Wang, A core–shell structure of polyaniline coated protonic titanate nanobelt composites for both Cr(VI) and humic acid removal, Polym. Chem. 7 (2016) 785–794.

[43] J. Wang, X. Wang, G. Zhao, G. Song, D. Chen, H. Chen, Polyvinylpyrrolidone and polyacrylamide intercalated molybdenum disul fi de as adsorbents for enhanced removal of chromium (VI) from aqueous solutions, Chem. Eng. J. 334 (2018) 569–578.

[44] T. Wen, J. Wang, S. Yu, Z. Chen, T. Hayat, X. Wang, Magnetic porous carbonaceous material produced from tea waste for efficient removal of As(V), Cr(VI), humic acid, and dyes, ACS Sustain. Chem. Eng. 5 (2017) 4371–4380.